Received August 1997
Revised December 1997
Accepted March 1998

Transient analysis of LE-VGF growth of compound semiconductors

Yasunori Okano, Susumu Sakai, Takahiro Morita and Jun Shimizu

Department of Materials Science and Chemical Engineering, Shizuoka University, Johoku, Hamamatsu, Japan

Introduction

Bulk single crystals of compound semiconductors such as GaAs and InP are very important materials for the substrates of various electronic devices. The Czochralski technique is widely used for the growth of these crystals. However, container crystal growth techniques, i.e. the vertical gradient freezing (VGF) and vertical Bridgman (VB) techniques are very promising because they can grow crystals without diameter control in a lower axial-thermal-gradient than that of the Czochralski method[1].

Components of compound semiconductor melts such as As and P are very easy to evaporate. Therefore, in order to grow high-quality crystals, it is required to suppress the volatilization and maintain the stoichiometry of the components during growth. From this point of view, the liquid encapsulated vertical Bridgman (LE-VB) technique[2] and the liquid encapsulated vertical gradient freezing (LE-VGF) technique[3] have been proposed. Recently, Matsumoto *et al.*[4] have successfully grown twin-free bulk single crystals of InP by the LE-VB technique with a flat bottom crucible and Okada *et al.*[5] have grown ZnSe single crystals by the LE-VB technique.

In order to grow high-quality single crystals, it is necessary to control the flow and temperature fields which affect the melt/crystal interface shape and segregation phenomena during crystal growth. However, it is impossible to observe and measure these phenomena during crystal growth because the crystal is grown in a crucible under high pressure. Therefore, numerical simulation is attractive for the establishment of the optimum furnace design and growth conditions, and many numerical studies have been reported[6]. A pseudo steady-state has been assumed in numerous studies[7-16]. Recently, three-dimensional calculations on the VB crystal growth system have been reported[17,18].

Kim and Brown have performed a transient analysis on the VGF[19] and VB[20,21] crystal growth systems by the finite element method. Kuppurao *et al.*

This work was partially supported by the Assistance of International Information Exchanges, TEPCO Research Foundation, and a Grant-in-Aid for Scientific Research (B) (No. 07305060) from the Japanese Ministry of Education, Science and Culture. The authors wish to thank S. Nishino for his help with the computer calculations.

International Journal of Numerical Methods for Heat & Fluid Flow
Vol. 8 No. 8, 1998, pp. 956-968.

have performed the transient analysis by the finite element method on the VB growth of CdZnTe crystal[22], and discussed the effect of the interrupted growth strategies on the melt/crystal interface shape in the VB growth of CdTe crystal[23]. Saitou and Hirata have analyzed the unsteady solidification problem without[24,25] and with[26] the melt convection by the finite difference method, but a crucible has not been considered and the radiative heat transfer has been ignored in their studies. Those transient analyses[19-26] have concerned the VGF or VB systems, which include no encapsulant. Only Lan and Ting[27] have performed the transient analyses on the liquid encapsulated vertical Bridgman (LE-VB) growth system by the finite volume method. They have studied the effect of the anisotropy of a pBN crucible on the growth speed and shape of the melt/crystal interface. The effect of the crucible on the interface shape has also been discussed in the VB[8,27] and LE-VB[28,29] systems by other researchers. Irizzary-Rivera and Seider[28] have showed that the thickness of the crucible is an important factor to control the melt/crystal interface shape.

This study concerns the LE-VGF growth of InP single crystals with a flat bottom crucible[4]. The transient analysis is performed to discuss the effect of the crucible thickness, the thermal conductivity of the crucible and the furnace temperature on the flow and thermal fields during growth.

Numerical analysis

Model description and governing equations

Figure 1 shows a basic configuration and coordinate system. The model consists of a crystal, melt, encapsulant, crucible and a carbon crucible holder. A flat bottom crucible which has been used in the previous experimental study[4] by one of the present authors is considered. The model includes the following assumptions:

(1) the system is radially symmetric;

(2) the melt is incompressible and Newtonian;

(3) the flow is laminar;

(4) the Boussinesq approximation can be adopted;

(5) the liquid encapsulated material is B_2O_3, which is completely transparent, and convection in the B_2O_3 is negligible because of high viscosity;

(6) the melt/crystal interface is at the melting point, T_m;

(7) the B_2O_3/melt and B_2O_3/ambient interfaces are flat and nondeformable;

(8) any changes in the volume and physical properties as a result of the melting are neglected; and

(9) the temperature of the furnace wall, T_a is constant. Under these assumptions, the governing equations in terms of stream function ψ, vorticity ω and temperature T are described as follows.

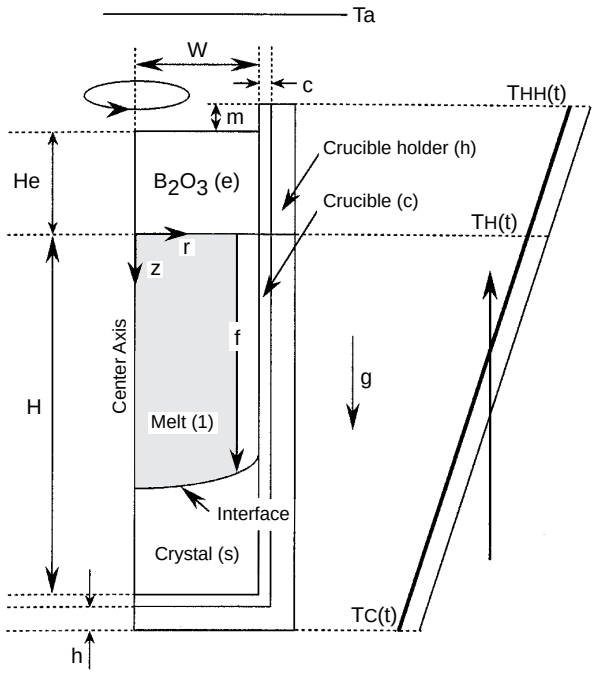

Figure 1.
Basic configuration and coordinate system

In the melt (l);

$$\frac{\partial \omega}{\partial t} + v_r \frac{\partial \omega}{\partial r} + v_z \frac{\partial \omega}{\partial r} - \frac{v_r}{r}\omega = \nu\left(\frac{\partial^2 \omega}{\partial r^2} + \frac{\partial^2 \omega}{\partial z^2} + \frac{1}{r}\frac{\partial \omega}{\partial r} - \frac{\omega}{r^2}\right) - \frac{\partial}{\partial r}(g\beta\Delta T_l) \quad (1)$$

$$\omega = \frac{\partial v_r}{\partial z} - \frac{\partial v_z}{\partial r} = \frac{1}{r}\frac{\partial^2 \psi}{\partial z^2} - \frac{1}{r^2}\frac{\partial \psi}{\partial r} + \frac{1}{r}\frac{\partial^2 \psi}{\partial r^2} \quad (2)$$

$$\frac{\partial T_l}{\partial t} + v_r \frac{\partial T_l}{\partial r} + v_z \frac{\partial T_l}{\partial z} = \alpha_l\left(\frac{\partial^2 T_l}{\partial r^2} + \frac{1}{r}\frac{\partial T_l}{\partial r} + \frac{\partial^2 T_l}{\partial z^2}\right) \quad (3)$$

where g, v_j, β and α are the gravitational acceleration, the velocity in the j-direction (j = r or z), the coefficient of thermal expansion of the melt and thermal diffusivity, respectively.

In the crystal (s), crucible (c), crucible holder (h) and encapsulant (e);

$$\frac{\partial T_i}{\partial t} = \alpha_i\left(\frac{\partial^2 T_i}{\partial r^2} + \frac{1}{r}\frac{\partial T_i}{\partial r} + \frac{\partial^2 T_i}{\partial z^2}\right) \quad (4)$$

where i = s, c, h or e.

The boundary conditions are given as follows,

Along the center axis (r = 0):

$$v_r = \frac{\partial v_z}{\partial R} = \frac{\partial T_i}{\partial r} = 0 \tag{5}$$

where i = l, s, c, h or e.

Along the upper surfaces ($z = -H_e$ for encapsulant, and $z = -(H_e+m)$ for the crucible and crucible holder), both radiative and convective heat transfer are considered, but the effect of view factor is ignored:

$$\lambda_i \frac{\partial T_i}{\partial z} = h(T_i - T_a) + \sigma\varepsilon_i(T_i^4 - T_a^4) \tag{6}$$

where i = e, c or h.

where λ, h, σ and ε are the thermal conductivity, convective heat transfer coefficient of ambient gas, Stefan-Boltzmann constant and emissivity, respectively.

Along the melt/encapsulant interface ($0 \leqq r \leqq W$, $z = 0$):

$$v_r = v_z = 0 \tag{7}$$

$$-\lambda_l \frac{\partial T_l}{\partial z} = \sigma\varepsilon_l(T_l^4 - T_a^4) \tag{8}$$

$$\lambda_l \frac{\partial T_l}{\partial z} = \lambda_e \frac{\partial T_e}{\partial z} \tag{9}$$

Along the melt/crystal interface ($0 \leqq r \leqq W$, $z = f(r)$):

$$v_r = v_z = 0 \tag{10}$$

$$T_l = T_s = T_m \tag{11}$$

$$\rho_s \Delta H \frac{\partial f}{\partial t} = \left(\lambda_s \frac{\partial T_s}{\partial z} - \lambda_l \frac{\partial T_l}{\partial z}\right)\left\{1 + \left(\frac{\partial f}{\partial r}\right)^2\right\} \tag{12}$$

Equation (12) is the energy balance along the melt/crystal interface and ΔH is the heat of fusion.

Along the melt/crucible interface ($r = W$, $0 \leqq z \leqq f(w)$):

$$v_r = v_z = 0 \tag{13}$$

$$\lambda_l \frac{\partial T_l}{\partial r} = \lambda_c \frac{\partial T_c}{\partial r} \tag{14}$$

Along the crucible/(encapsulant, crystal or crucible holder) interfaces:

$$\lambda_i \frac{\partial T_i}{\partial r} = \lambda_c \frac{\partial T_c}{\partial r} \qquad \text{(for the side wall)} \tag{15}$$

where, i = e, s or h

$$\lambda_i \frac{\partial T_i}{\partial z} = \lambda_c \frac{\partial T_c}{\partial z} \qquad \text{(for the bottom wall)} \tag{16}$$

where, i = s or h.

Along the inside surface of the crucible ($-(H_e+m) \leqq z \leqq -H_e$):

$$\frac{\partial T_c}{\partial r} = 0 \tag{17}$$

Along the bottom surface of the crucible holder (z = H+c+h):

$$\frac{\partial T_h}{\partial z} = 0 \tag{18}$$

Along the side wall of the crucible holder (r = W+c+h):

$$T = T(z,t). \tag{19}$$

Coordinate transformation

In order to treat a curvature interface, the boundary fixing method[30] was used. The governing equations and boundary conditions were transformed by the following variables;

In the melt:

$$\eta = \frac{Z}{F(R,\tau)}. \tag{20}$$

In the crystal:

$$\xi = \frac{Z - F(R,\tau)}{A - F(R,\tau)} \tag{21}$$

where Z, F, R and τ are dimensionless values, defined as z/W, f/W, r/W and $t\alpha_l/W^2$, respectively.

The transformed governing equations in a dimensionless form are described as follows:

In the melt:

$$\frac{\partial\Omega}{\partial\eta}\frac{\partial\eta}{\partial\tau}+\frac{\partial\Omega}{\partial\tau}+V_R\left(\frac{\partial\eta}{\partial R}\frac{\partial\Omega}{\partial\eta}+\frac{\partial\Omega}{\partial R}\right)+V_Z\frac{\partial\eta}{\partial Z}\frac{\partial\Omega}{\partial\eta}-\frac{\Omega}{R}V_R$$

$$=\mathrm{Pr}\left[\left\{\left(\frac{\partial\eta}{\partial R}\right)^2+\left(\frac{\partial\eta}{\partial Z}\right)^2\right\}\frac{\partial^2\Omega}{\partial\eta^2}+2\frac{\partial\eta}{\partial R}\frac{\partial^2\Omega}{\partial R\partial\eta}+\frac{\partial^2\eta}{\partial R^2}\frac{\partial\Omega}{\partial\eta}+\frac{\partial^2\Omega}{\partial R^2}+\frac{1}{R}\left(\frac{\partial\eta}{\partial R}\frac{\partial\Omega}{\partial\eta}+\frac{\partial\Omega}{\partial R}\right)-\frac{\Omega}{R^2}\right]$$

$$+\frac{\mathrm{Gr}\cdot\mathrm{Pr}^2}{A^3}\left(\frac{\partial\eta}{\partial R}\frac{\partial\theta_1}{\partial\eta}+\frac{\partial\theta_1}{\partial R}\right) \tag{22}$$

$$R\Omega=\left\{\left(\frac{\partial\eta}{\partial R}\right)^2+\left(\frac{\partial\eta}{\partial Z}\right)^2\right\}\frac{\partial^2\Psi}{\partial\eta^2}+2\frac{\partial\eta}{\partial R}\frac{\partial^2\Psi}{\partial R\partial\eta}+\frac{\partial^2\eta}{\partial R^2}\frac{\partial\Psi}{\partial\eta}+\frac{\partial^2\Psi}{\partial R^2}-\frac{1}{R}\left(\frac{\partial\eta}{\partial R}\frac{\partial\Psi}{\partial\eta}+\frac{\partial\Psi}{\partial R}\right) \tag{23}$$

$$\frac{\partial\theta_1}{\partial\eta}\frac{\partial\eta}{\partial\tau}+\frac{\partial\theta_1}{\partial\tau}+V_R\left(\frac{\partial\eta}{\partial R}\frac{\partial\theta_1}{\partial\eta}+\frac{\partial\theta_1}{\partial R}\right)+V_Z\frac{\partial\eta}{\partial Z}\frac{\partial\theta_1}{\partial\eta}$$

$$=\left\{\left(\frac{\partial\eta}{\partial R}\right)^2+\left(\frac{\partial\eta}{\partial Z}\right)^2\right\}\frac{\partial^2\theta_1}{\partial\eta^2}+2\frac{\partial\eta}{\partial R}\frac{\partial^2\theta_1}{\partial R\partial\eta}+\frac{\partial^2\eta}{\partial R^2}\frac{\partial\theta_1}{\partial\eta}+\frac{\partial^2\theta_1}{\partial R^2}+\frac{1}{R}\left(\frac{\partial\eta}{\partial R}\frac{\partial\theta_1}{\partial\eta}+\frac{\partial\theta_1}{\partial R}\right) \tag{24}$$

where Ω, ψ and θ are dimensionless vorticity, dimensionless stream function and dimensionless temperature, respectively. Dimensionless velocities are defined as

$$V_R=\frac{1}{R}\frac{\partial\eta}{\partial Z}\frac{\partial\Psi}{\partial\eta}\quad\text{and}\quad V_Z=-\frac{1}{R}\left(\frac{\partial\eta}{\partial R}\frac{\partial\Psi}{\partial\eta}+\frac{\partial\Psi}{\partial R}\right). \tag{25}$$

In equation (22), Gr and A denote the Grashof number and the aspect ratio, respectively, defined as

$$\mathrm{Gr}=\frac{g\beta(TH-Tm)W^3}{\nu^2} \tag{26}$$

$$A=H/W. \tag{27}$$

In the crystal:

$$\frac{\partial\theta_s}{\partial\xi}\frac{\partial\xi}{\partial\tau}+\frac{\partial\theta_s}{\partial\tau}=\frac{\alpha_s}{\alpha_1}\left[\left\{\left(\frac{\partial\xi}{\partial R}\right)^2+\left(\frac{\partial\xi}{\partial Z}\right)^2\right\}\frac{\partial^2\theta_s}{\partial\xi^2}+2\frac{\partial\xi}{\partial R}\frac{\partial^2\theta_s}{\partial R\partial\xi}\right.$$

$$\left.+\frac{\partial^2\xi}{\partial R^2}\frac{\partial\theta_s}{\partial\xi}+\frac{\partial^2\theta_s}{\partial R^2}+\frac{1}{R}\left(\frac{\partial\xi}{\partial R}\frac{\partial\theta_s}{\partial\xi}+\frac{\partial\theta_s}{\partial R}\right)\right] \tag{28}$$

The energy-balance along the melt/crystal interface, equation (12), is transformed into

$$\frac{\partial F}{\partial \tau} = \mathrm{Ste}\left(\frac{\lambda_s}{\lambda_l}\frac{\partial \xi}{\partial Z}\frac{\partial T_s}{\partial \xi} - \frac{\partial \eta}{\partial Z}\frac{\partial T_l}{\partial \eta}\right)\left\{1 + \left(\frac{\partial F}{\partial R}\right)^2\right\} \quad (29)$$

Here Ste is the Stefan number, defined as

$$\mathrm{Ste} = \frac{\rho_L Cp(T_H - T_m)}{\rho_S \Delta H} \quad (30)$$

In the crucible (c), crucible holder (h) and encapsulant (e);

$$\frac{\partial \theta_i}{\partial \tau} = \frac{\alpha_i}{\alpha_l}\left(\frac{\partial^2 \theta_i}{\partial R^2} + \frac{1}{R}\frac{\partial \theta_i}{\partial R} + \frac{\partial^2 \theta_i}{\partial Z^2}\right) \quad (31)$$

where i = c, h or e.

Numerical procedure

Equations (22)-(25), (28) and (31) and transformed boundary conditions such as equation (29) were discretized by the finite difference method. The third-order upwind difference method[31] and the second-order central difference method were applied to the inertia and viscous terms, respectively. A fully implicit scheme was employed for time stepping. The discretized governing equations and boundary conditions were solved by the SOR method. The number of mesh is shown in Table I.

Physical properties and system parameters

Physical properties of the melt and crystal of InP, pBN and B_2O_3 are shown in the paper by Lan and Ting[27]; and 0.55, 0.8 and 0 were used as values of emissivity of InP melt, pBN and B_2O_3, respectively. The size of the system is shown in Table II. The size corresponds to that of the previous experimental setup for InP single crystal growth[4]. The temperature distribution along the crucible wall ($\partial T/\partial z$) is –1.5°C/mm, and the temperature lowering rate is 3°C/h.

	Radial	Axial
Encapsulant	73	49
Melt	73	75
Crystal	73	25
Crucible	0~14[a]	157~170[a]
Crucible holder	13	169~182[a]

Note: [a]Thickness of the crucible was changed

Table I.
Number of mesh

Results and discussion

Figure 2 shows the flow pattern (left-hand side) and isothermal lines (right-hand side) in every 200 min when the thickness of the pBN crucible is 2mm. Natural convection, due to the radial temperature gradient is generated in the melt and flows clockwise. As the crystal grows, the flow in the melt is suppressed, and the melt/crystal interface shape changes from convex toward the crystal to convex toward the melt. This behavior is in good agreement with the experimentally observed one[32].

Figure 3 shows the effect of the crucible thickness on the flow and thermal fields at the initial condition, i.e. t = 0. Figure 3(a) shows the case ignoring both the crucible and crucible holder, and (b) shows the case where the thickness of the

Inner radius of the crucible, W	24.0mm
Length of crystal, H	73.3mm
Depth of encapsulant, He	25.0mm
Thickness of the crucible, c	0~4mm
Thickness of the crucible holder	4mm
m	5mm

Table II.
Size of system

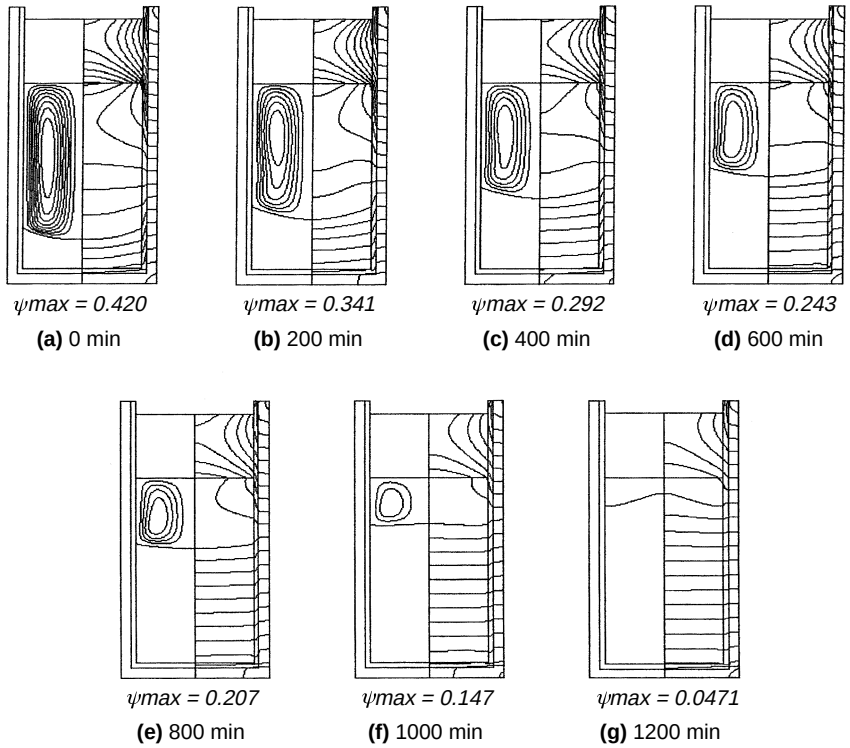

Figure 2.
Flow pattern (left-hand side) and isothermal lines (right-hand side) at 200 min intervals when the thickness of pBN crucible is 2mm. $\Delta\psi = 0.05$, $\Delta T = 0.1$ and Ta = 1,052°C

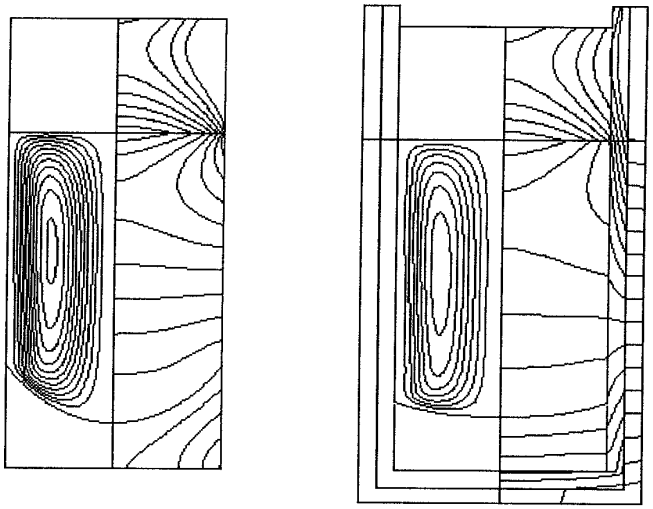

Figure 3.
Effect of crucible thickness on the flow and temperature fields at the initial condition (a) without crucible and crucible holder, and (b) crucible thickness of 4mm. $\Delta\psi = 0.05$, $\Delta T = 0.1$ and Ta = 1,052°C

pBN crucible is 4mm. When the crucible and crucible holder are ignored, the interfacial deflection is larger than that in the case in which the crucible and crucible holder are considered. A pBN crucible is synthesized by the CVD method and has strong thermal conductivity anisotropy. The thermal conductivity parallel to the crucible wall is much higher than the perpendicular one[29]. Therefore, the heat flow perpendicular to the crystal bottom is suppressed by the pBN crucible and the radial thermal gradient in the crystal becomes small as shown in Figure 3(b). Consequently, the interfacial deflection becomes small.

Figure 4 shows the effect of the crucible thickness on the transient behavior. Figure 4(a) shows the growth rate along the center axis (r = 0) and (b) shows the dimensionless interfacial deflection, δ(= $\Delta F/W$). ΔF is the deviation from the flat interface at r = 0. Positive and negative values of δ denote the convex and concave interfacial shape toward the melt, respectively. As shown in Figure 4, the growth rate along the center axis is not constant although the temperature lowering rate is constant. A pBN crucible enhances the heat flow along the crucible wall as shown in Figure 3(b). Therefore, a thicker crucible decreases the maximum temperature in the melt in spite of the same temperature along the side wall. Consequently, the growth rate increases when a thicker crucible is used. However, the growth rate in the early stage of growth is also affected by the initial interfacial shape and is complicated.

Figure 5 shows the effect of the thermal conductivity of the crucible when the crucible thickness is 2 mm. λ_R and λ_Z are thermal conductivities perpendicular and parallel to the crucible wall, respectively. Anisotropic thermal conductivity corresponds to a pBN crucible. The thermal conductivity of the crucible has a considerable effect on the interfacial deflection. By using a crucible with lower thermal conductivity, a small deflective interface shape can be obtained.

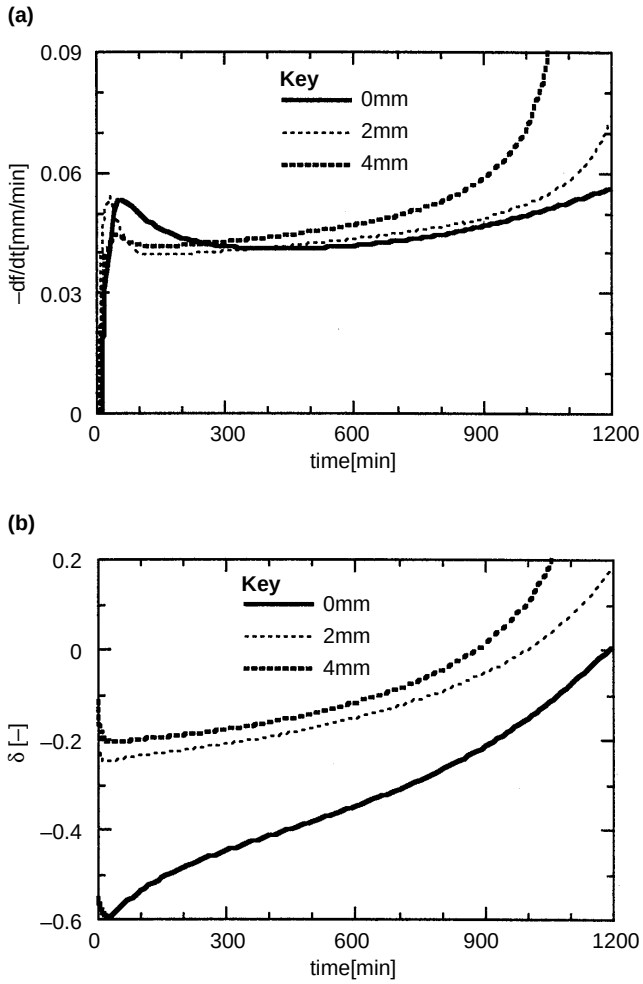

Figure 4. Effect of crucible thickness on (a) the growth rate and (b) dimensionless interfacial deflection when Ta = 1,052°C

Figure 6 shows the effect of furnace wall temperature,Ta, on the temperature distribution in the crucible when the thickness of pBN crucible is 2 mm and t = 700 min. Bold lines show the melt/crystal interface. When Ta is low, heat flow from the melt to the furnace is enhanced and the melt/crystal interface shape becomes flat.

Conclusion

The transient analysis for the bulk single crystal growth of InP by the liquid encapsulated vertical gradient freezing method with a flat bottom crucible was performed by the finite difference method with the boundary fixing method, and the following results were obtained:

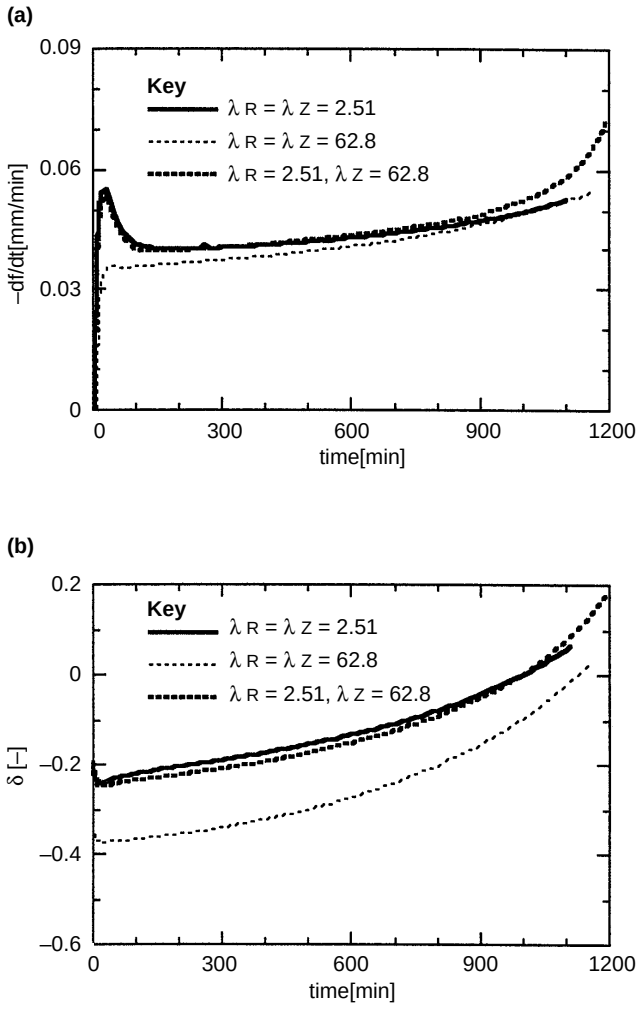

Figure 5.
Effect of thermal conductivity of the crucible on (a) the growth rate and (b) dimensionless interfacial deflection when Ta = 1,052°C and c = 2mm

(1) Crystal growth rate at the center axis is not constant during the crystal growth although the temperature lowering rate along the side wall of crucible is constant.

(2) The crucible thickness and thermal conductivity of the crucible are important factors which influence the shape of the crystal/melt interface and crystal growth rate. The crystal with a flatter interface shape, which is favorable to obtain high quality crystal, can be grown using a thick crucible with low thermal conductivity.

(3) Crystals which are flat or convex toward the melt can be grown in the furnace with the low temperature wall.

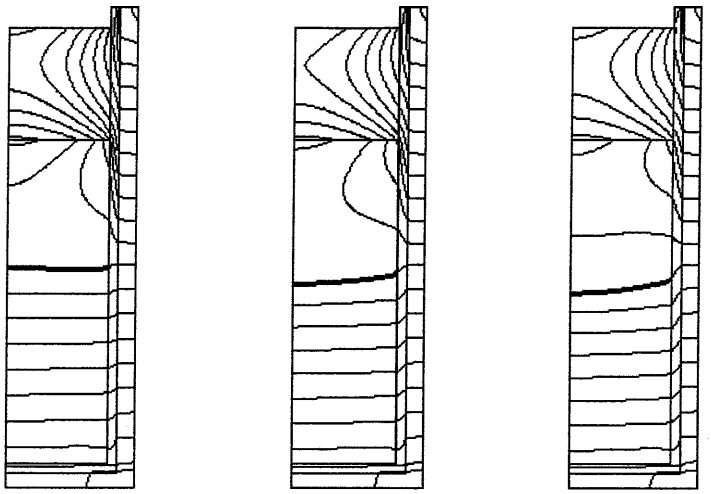

δ = – 0.0591
(a) Ta = 1032°C

δ = – 0.0967
(b) Ta = 1042°C

δ = – 0.1389
(c) Ta = 1052°C

Figure 6.
Effect of temperature of furnace wall on the temperature distribution in the crucible. pBN crucible, c = 2mm and t = 700 min. ΔT = 0.1

References

1. Monberg, E., "Bridgman and related growth techniques", in Hurle, D.T.J. (Ed.), *Handbook of Crystal Growth,* Elsevier, Amsterdam, Vol. 2, 1994, Ch. 2, pp. 53-97.
2. Hoshikawa, K., Nakanishi, H., Kohda, H. and Sasaura, M., "Liquid encapsulated, vertical Bridgman growth of large diameter, low dislocation density, semi-insulating GaAs", *J. Crystal Growth,* Vol. 94, 1989, pp. 643-50.
3. Monberg, E.M., Brown, H. and Bonner, C.E., "The dynamic gradient freeze growth of InP", *J. Crystal Growth,* Vol. 94, 1989, pp. 109-14.
4. Matsumoto, F., Okano, Y., Yonenaga, I., Hoshikawa, K. and Fukuda, T., "Growth of twin-free <100> InP single crystals by the liquid encapsulated vertical Bridgman technique", *J. Crystal Growth*, Vol. 132, 1993, pp. 348-50.
5. Okada, H., Kawanaka, T. and Ohmoto, S., "Melt growth of ZnSe single crystals with B_2O_3 encapsulant: the role of solid-solid phase transformation on macro defect generation in ZnSe crystals", *J. Crystal Growth*, Vol. 172, 1997, pp. 361-9.
6. Dupret, F. and Van Den Bogaert, N., "Modeling Bridgman and Czochralski growth", in Hurle, D.T.J. (Ed.), *Handbook of Crystal Growth,* Elsevier, Amsterdam, Vol. 2, 1994, Ch. 15, pp. 877-1010.
7. Chang, C.J. and Brown, R.A., "Radial segregation induced by natural convection and melt/solid interface shape in vertical Bridgman growth", *J. Crystal Growth*, Vol. 63, 1983, pp. 343-64.
8. Jasinski, T. and Witt, A.F., "On control of the crystal-melt interface shape during growth in a vertical Bridgman configuration", *J. Crystal Growth,* Vol. 71, 1985, pp. 295-304.
9. Adornato, P.M. and Brown, R.A., "Convection and segregation in directional solidification of dilute and non-dilute binary alloys: effect of ampoule and furnace design", *J. Crystal Growth,* Vol. 80, 1987, pp. 292-304.
10. Kim, D.H. and Brown, R.A., "Models for convectional and segregation in the growth of HgCdTe by the vertical Bridgman method", *J. Crystal Growth*, Vol. 96, 1989, pp. 609-27.
11. Crochet, M.J., Dupret, F., Ryckmans, Y., Geyling, F.T. and Monberg, E.M., "Numerical simulation of crystal growth in a vertical Bridgman furnace", *J. Crystal Growth*, Vol. 97, pp. 173-85.

12. Yao, M., Chait, A., Fripp, A.L. and Debnam, W.J., "Numerical simulation of Bridgman crystal growth of PbSnTe in microgravity", *Microgravity Sci. Technol.*, Vol. 8, 1995, pp. 214-25.
13. Kuppurao, S., Brandon, S. and Derby, J.J., "Modeling the vertical Bridgman growth of cadmium zinc telluride, I. Quasi-steady analysis of heat transfer and convection", *J. Crystal Growth,* Vol. 155, 1995, pp. 93-102.
14. Lan, C.W. and Ting, C.C., "Computer simulation of liquid encapsulated vertical Bridgman crystal growth: Pseudo steady-state calculations", *Int. J. Meth. Heat Fluid Flow*, Vol. 6, 1996, pp. 3-24.
15. Kuppurao, S. and Derby, J.J., "Designing thermal environments to promote convex interface shapes during the vertical Bridgman growth of cadmium zinc telluride", *J. Crystal Growth*, Vol. 172, 1997, pp. 350-60.
16. Ouyang, H. and Shyy, W., "Numerical simulation of CdTe vertical Bridgman growth", *J. Crystal Growth*, Vol. 173, 1997, pp. 352-66.
17. Xiao, Q., Kuppurao, S., Teckel, A. and Derby, J.J., "On the effect of ampoule tilting during vertical Bridgman growth: three-dimensional computations via a massively parallel, finite element method", *J.Crystal Growth*, Vol. 167, 1997, pp. 292-304.
18. Liang, M.C. and Lan, C.W., "Three-dimensional convection and solute segregation in vertical Bridgman crystal growth", *J. Crystal Growth*, Vol. 167, 1997, pp. 320-32.
19. Kim, D.H. and Brown, R.A., "Transient simulations of convection and solute segregation of GaAs growth in gradient freeze furnace", *J. Crystal Growth*, Vol. 109, 1991, pp. 66-74.
20. Brown, R.A. and Kim, D.H., "Modeling of directional solidification: from Scheil to detailed numerical simulations", *J. Crystal Growth*, Vol. 109, 1991, pp. 50-65.
21. Kim, D.H. and Brown, R.A., "Modeling of dynamics of HgCdTe growth by the vertical Bridgman method", *J. Crystal Growth*, Vol. 114, 1991, pp. 411-34.
22. Kuppurao, S., Brandon, S. and Derby, J.J., "Modeling the vertical Bridgman growth of cadmium zinc telluride, II.Transient analysis of zinc segregation", *J. Crystal Growth*, Vol. 155, 1995, pp. 103-11.
23. Kuppurao, S., Brandon, S. and Derby, J.J., "Analysis of interrupted growth strategies for cadmium telluride in an unseeded vertical Bridgman system", *J. Crystal Growth*, Vol. 158, 1996, pp. 459-70.
24. Saitou, M. and Hirata, A., "Numerical calculation of two-dimensional unsteady solidification problem", *J. Crystal Growth*, Vol. 113, 1991, pp. 147-56.
25. Saitou, M. and Hirata, A., "Two-dimensional unsteady solidification problem calculated by using the boundary-fitted coordinate system", *J. Comp. Phys.*, Vol. 100, 1992, pp. 188-96.
26. Saitou, M. and Hirata, A., "A numerical method for solving the two-dimensional unsteady solidification problem with the motion of melt by using the boundary-fitted co-ordinate system", *Int. J. Numer. Meth. Eng.*, Vol. 36, 1993, pp. 403-16.
27. Lan, C.W. and Ting, C.C., "Numerical investigation on the batch characteristics of liquid encapsulated vertical Bridgman crystal growth", *J. Crystal Growth*, Vol. 149, 1995, pp. 175-86.
28. Irizzary-Rivera, R. and Seider, W.D., "Optimal interface for the Bridgman crystallization process", *Numer. Heat Transfer, Part A*, Vol. 29, 1996, pp. 227-42.
29. Suzuki, T., Okano, Y., Hoshikawa, K. and Fukuda, T., "Heat transfer during GaAs growth of bulk single crystal by the liquid encapsulated vertical Bridgman technique", *J. Crystal Growth,* Vol. 128, 1993, pp. 435-8.
30. Saitoh, T., "Numerical method for multi-dimensional freezing problems in arbitrary domains", *Trans. ASME, J. Heat Transfer*, Vol. 100, 1978, pp. 294-9.
31. Kawamura T. and Kuwahara, K., "Computation of high Reynolds number flow around a circular cylinder with surface roughness", AIAA Paper 84-0340, 1984.
32. Rudolph, P., Matsumoto, F. and Fukuda, T., "Studies on interface curvature during vertical Bridgman growth of InP in a flat-bottom container", *J. Crystal Growth,* Vol. 158, 1996, pp. 43-8.